Optimization of external coupling and light emission in organic light-emitting devices: modeling and experiment

M.-H. Lu[a) and J. C. Sturm[b)]
Department of Electrical Engineering, Center for Photonics and Optoelectronic Materials,
Princeton University, Princeton, New Jersey 08544

The emission of light and external coupling after the appropriate excitons have been formed in the organic light-emitting devices (OLEDs) has been investigated. The internally emitted light can be classified into three modes: externally emitted, substrate waveguided, and indium–tin–oxide (ITO)/ organic waveguided. A combined classical and quantum mechanical microcavity model is used to calculate the distribution of light emission into these three modes in an OLED on planar substrates. The ITO/organic modes maybe suppressed due to the thinness of the ITO/organic layers. Consequently, as much as over 50% of the internally generated light is emitted externally in some structures, much greater than the ~20% figure given by classical ray optics. This model is used to examine how this distribution varies with exciton to cathode distance, the thickness of the ITO layer, and the index of refraction of the substrate. It can also be applied to OLEDs on shaped substrates where an increase in the total external emission up to a factor of 2.3 has been demonstrated. The numerical results agree well with experimentally measured far-field intensity profiles, edge emissions, and increase in external emission due to shaped substrates. Finally, based on these results, we discuss different approaches to device optimization, depending on the fluorescence efficiency of the emitter and whether a shaped substrate is used. © *2002 American Institute of Physics.* [DOI: 10.1063/1.1425448]

I. INTRODUCTION

Organic light-emitting devices (OLEDs) have attracted wide interest due to their applications in flat panel displays. One critical figure of merit for OLEDs is the electroluminescence (EL) efficiency η_{EL}^{ext} (externally emitted photons/ electron). It is the product of the internal quantum efficiency η_{EL}^{int} (internally emitted photons/electron), and the external coupling efficiency η_{cp}^{ext}, the fraction of thus internally emitted photons that actually escape outside. In this article, we investigate the emission of light after the appropriate exciton has been formed in the OLED and calculate η_{cp}^{ext} and its dependency on the OLED structure, including backside substrate patterning and high index of refraction substrates.

The article is organized as follows: in Sec. II the device architecture used in both simulation and experiments is described, and the combined classical and quantum mechanical microcavity (CCQMM) model is developed before presenting selected numerical results. Experimental procedure and setup are described in Sec. III. Experimental results, discussions, and device optimization approaches are presented in Sec. IV. The conclusions are in Sec. V.

II. THEORY

A. OLED structure

A schematic diagram of the OLED structure used in both modeling and experiments is shown in Fig. 1. The device consists of a glass substrate that is made of either soda lime glass (standard substrate $n_{glass1} = 1.51$) or Schott SFL57 glass (high-index glass $n_{glass2} = 1.85$), an indium–tin–oxide (ITO) ($n_{ITO} = 1.8 – 2.0$) anode, a poly-(N-vinylcarbazole) (PVK) ($n_{PVK} = 1.67$) hole transporting layer, a tris-(8-hydroxyquinoline) aluminum (Alq$_3$, $n_{Alq} = 1.71$) electron transporting and emitting layer, and a 30–50 nm Mg:Ag (10:1) cathode followed by a 150 nm Ag cap. The EL spectrum shows that the emission comes exclusively from the Alq$_3$ layer. The OLED microcavity is confined by the reflecting cathode and the leaky ITO/glass interface.

The emitted light can be classified into three modes: the external modes that escape the substrate, the substrate-waveguided modes that are trapped in the glass substrate by total internal refraction (TIR) at the glass/air interface, and the ITO/organic-waveguided modes that are trapped by TIR at the ITO/glass interface (Fig. 2).

B. Background and other theoretical treatments

Due to the index mismatch between the emitting layer and air, a large fraction of the light is trapped in the glass, ITO, and organic layers. This effect is well known in inorganic semiconductor light emitting diodes, where the external coupling efficiency is estimated by classical ray optics to be $1/2n^2$ for large n.[1,2] However, the multilayers of an OLED represent a different photonic structure that is not well described by classical ray optics. The ray optics result leads to an unrealistically high estimate for the internal quantum efficiency in some efficient devices.[3,4] In addition, several groups have reported dependence of the far-field emission pattern on the thickness of the organic layer, which is not explained by the classical theory.[5,6]
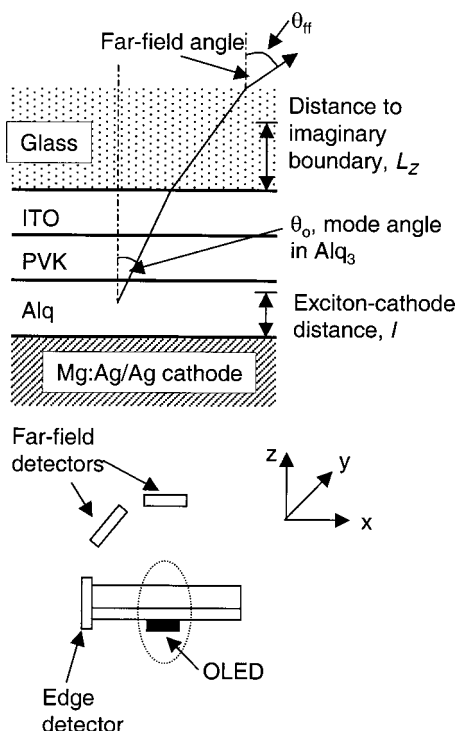
FIG. 1. Schematic diagram of the setup for modeling and experiments.

The behavior of radiating molecules in an optical micro-cavity is a general problem that can be approached in two ways: one based on classical electrodynamics and one based on quantum mechanics. Using a classical approach, many groups have examined the far-field emission characteristics as a function of the OLED layer structure using wave optics and a transfer matrix formalism.[7–12] Recently, the EL pattern of polymer LEDs was found to be accurately described by a half-space dipole model that accounts for optical interference effects due to the metal cathode.[13] The most comprehensive classical treatment of the general problem is that presented by Chance et al.,[14] where the radiating molecule is modeled as a classical oscillating dipole and the radiation fields in the layered media are described by a dyadic Green's function. Some of their earlier work was based on a Hertzian vector approach that has recently been applied to OLEDs.[15–17] They have shown that the Green's function method is completely equivalent and more easily applied to general stratified

FIG. 2. Three radiative modes in OLEDs: (I) external modes, (II) substrate modes, and (III) ITO/organic modes.

media.[14] This classical treatment provides a complete description of radiation in the OLED microcavity and has been combined with transport theory to successfully calculate the charge recombination and exciton emission zones of a single-layer polymer OLED.[18] From a quantum mechanical point of view, Ujihara presented field quantization of a one-dimensional optical cavity with external coupling in an early article.[19] Similar quantum mechanical treatments were used to describe the change in rate, spectrum, and directionality of emission from radiative dipoles in III–V semiconductor microcavities.[20,21]

The CCQMM model was developed by Bulović et al.[22] In the QM treatment, the electromagnetic field in the layered microcavity is represented by the sum of eigenmodes of the cavity; the radiating molecule is modeled as a dipole; and the transition probability into each mode is given by Fermi's golden rule. It has the advantage that the transition rates into the external, substrate, and ITO/organic modes are computed separately. The shortcoming of the quantum mechanical approach is that it does not account for the energy transfer from the dipole to the metal electrodes. However, it was shown by Chance et al. that this energy transfer arises exclusively from the near field of the dipole,[14] so it does not affect the shape of the normalized far-field intensity patterns. In the model developed by Bulović et al., the QM microcavity treatment is augmented by the Green's function analysis which is more convenient in computing the total rate of energy loss, hence the dipole lifetime in layered media.[22] We will use this model to determine the distribution of luminous flux emitted into the three above-mentioned modes and to examine its dependence on the thickness and material constants of the constituent layers. Numerical results will be compared with measured intensity profiles and edge emission data.

C. Exciton recombination process

Both EL and photoluminescence (PL) are due to the radiative recombination of Frenkel excitons within the organic layers.[23] Since the quantum mechanical approach is based on the dipole approximation, and the classical analysis models the recombining excitons as oscillating dipoles we will use the terms "exciton" and "dipole" interchangeably. Our discussion is initially based on the emitter/electron transport material Alq_3, although the extension to doped systems is straightforward.

The intrinsic rates of exciton recombination can be determined from the PL quantum efficiency η_{PL} of a thick film[22]

$$\eta_{PL} = W_0/(W_0 + W_{NR}^0), \tag{1}$$

where W_0 is the intrinsic rate of radiative decay and W_{NR}^0 is the intrinsic rate of nonradiative decay due to internal conversion and intersystem crossing. The PL efficiency of Alq_3 has been accurately measured to be $32\% \pm 2\%$.[24] For an exciton placed inside the OLED microcavity, the total recombination rate is

$$W_{TOT} = W_R + W_{ET} + W_{NR},$$
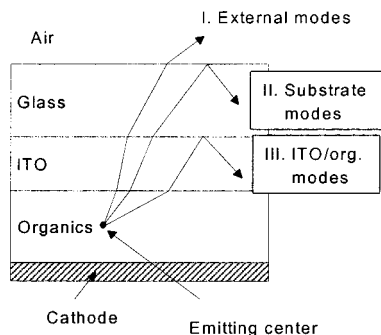$$W_R = W_{ext} + W_{sub} + W_{IO}, \tag{2}$$

where the rate of radiative decay W_R is the sum of the decay rates of the external, substrate, and ITO/organic modes. W_{ET} denotes the rate of energy transfer to the metallic cathode via nonradiative dipole–metal transfer and excitation of surface plasmons. W_{NR} again denotes the rate of nonradiative decay of the exciton, which is assumed to be unaffected by the placement in the microcavity, thus $W_{NR} = W_{NR}^0$.

The fraction of internally generated photons that are emitted externally is given by the external coupling efficiency $\eta_{cp}^{ext} = W_{ext}/W_R$, which is commonly held to be ~20% by ray optics. Also of great interest is the number of photons emitted externally for every singlet exciton created $\eta_{exciton} = W_{ext}/W_{TOT}$, which takes the nonradiative decay into account; consequently, it is a better measure of the external emission from the exciton in the microcavity. This can be seen more clearly if we let τ denote the total lifetime of the exciton. The amount of radiation each exciton emits into the external modes is given by $W_{ext}\tau = W_{ext}/W_{TOT} = \eta_{exciton}$. Various efficiency measures are related to each other as follows:

$$\eta_{EL}^{ext} = \eta_{EL}^{int}\eta_{cp}^{ext} = \gamma r_{st}\eta_{exciton},$$
$$\eta_{exciton} = \eta_R\eta_{cp}^{ext}, \tag{3}$$

where γ is the number of exciton forming events per electron flowing through the OLED, r_{st} is the portion of singlet excitons, and $\eta_R = W_R/W_{TOT}$ is the probability of radiative decay of the singlet excitons. It can be seen form Eq. (3) that the exact value of $\eta_{exciton}$ as a function of the emitter location in the cavity is critical in extracting the ratio of singlet/triplet excitons.[13,25]

Backside substrate patterning has been shown to increase the external emission by converting some of the substrate modes into external modes.[26–28] This increase in external quantum efficiency will be modeled and compared with experiments in this article. The conversion of substrate modes into external modes can be accounted for by replacing W_{ext} with $(W_{ext} + \beta W_{sub})$ in the efficiency calculations, where $1 > \beta > 0$ is the conversion efficiency.[29,30]

D. Radiative modes

The recombining exciton is modeled as a two-level system whose transition rate is given by Fermi's golden rule:

$$f = \frac{2\pi}{h}\sum_n |\langle m|\boldsymbol{\mu}\cdot\mathbf{E}(\mathbf{k},z)|n\rangle|^2\delta(E_n - E_m - h\nu), \tag{4}$$

where $\boldsymbol{\mu}$ is the dipole moment and $\mathbf{E}(\mathbf{k},z)$ is the electrical field for mode $\mathbf{k}$ at the location of the dipole; E_m and E_n are the energies of the initial and final exciton states; and $h\nu$ is the energy of the photon emitted. The total transition rate is obtained by summing over all $\mathbf{k}$, and ν. The OLED microcavity consists of, in sequence, the reflective cathode, the Alq$_3$ layer, the PVK layer, the ITO layer, ending in the glass substrate. Following Ujihara[19] and Deppe and Lei,[20] we place an imaginary upper boundary a distance L_Z away from the ITO/glass interface (Fig. 1), solve for all the modes, and later let L_Z tend to infinity. This treatment has the advantage that all modes become normalizable. Since the glass substrate is thick, the transmission from glass to air is handled by ray optics.[2,13] On the other hand, the ITO/organic layers are thin compared with the visible wavelengths, so the ITO/organic modes are discrete. The wave vectors $\mathbf{k}$ for these modes are described by transcendental equations that are solved numerically for both the TE and TM polarizations.[31]

The electric field is determined by the microcavity structure:

$$\mathbf{E}_{\mathbf{k}}^{TE} = \mathbf{A}(\mathbf{k})\sin^2(k_{oz}l)\mathbf{x},$$
$$\mathbf{E}_{\mathbf{k}}^{TM} = \mathbf{B}(\mathbf{k})\cos^2\theta_o\sin^2(k_{oz}l)\mathbf{y}$$
$$+ \mathbf{C}(\mathbf{k})\sin^2\theta_o\cos^2(k_{oz}l)\mathbf{z}, \tag{5}$$

where $\mathbf{A}(\mathbf{k})$, $\mathbf{B}(\mathbf{k})$, and $\mathbf{C}(\mathbf{k})$ are functions of material constants and $\mathbf{k}$; k_{oz} is the z component of the wave vector in the emitting layer; l is the dipole–cathode distance; and θ_o is the angle of the mode in the emitting layer. Here, the cathode is taken to be a perfect reflector. For spontaneous emission, the electric fields are normalized such that the energy in each mode is equal to that of a single photon. Near an antinode in the electric field where the $\sin^2(k_{oz}l)$ terms are maximized, the TE and first half of the TM radiation, both of which arise from the in-plane component of the electric field, are maximized. Near a node in the electric field, the second half of the TM radiation, which arises from the normal component of the electric field, is maximized, leading to a large in-plane TM component. We call the two components in the TM radiation the antinodal and nodal contribution, respectively.

Due to the high density of modes in the external and substrate modes, the sum in Eq. (7) may be replaced by an integral in the usual way: $\Sigma_{\mathbf{k}} \Rightarrow \int(\text{mode volume})^{-1}d\mathbf{k}$. On the other hand, the ITO/organic waveguide can support at most a couple of modes. The sum in Eq. (7) is then transformed into a two dimensional integral in the $k_x - k_y$ plane, and a discreet sum in k_z.

The excitons are assumed to be generated at the Alq$_3$/PVK interface and then diffuse into the Alq$_3$ layer. Tang and co-workers found the exciton diffusion length to be 20 nm, from examining the EL of an Alq$_3$ based device with varying dye-doped regions.[32] Throughout this work, we also assume the exciton recombination profile to be the same as the diffusion profile and use the same characteristic decay length. To calculate the intensity as a function of the mode angle in Alq$_3$, $I(\theta)$, the radiation from an exciton at a single point in space and at a single wavelength $I_{single}(\theta,\lambda,l)$ is weighted by the PL spectrum of Alq$_3$ and the exciton recombination profile which we assume decays exponentially from the PVK/Alq$_3$ interface with a characteristic length $L_D = 20$ nm:

$$I(\theta) = \frac{\int\int I_{single}(\theta,\lambda,l)P(\lambda)e^{-(d_o-l)/L_D}d\lambda\ dl}{\int P(\lambda)d\lambda\int e^{-(d_o-l)/L_D}dl}, \tag{6}$$

where $P(\lambda)$ is the Alq$_3$ PL spectrum, l is the dipole–cathode distance, and d_o is the thickness of the Alq$_3$ layer.

E. Energy transfer to the cathode

In this section we discuss the nonradiative energy transfer that arises from the near-field interaction between the
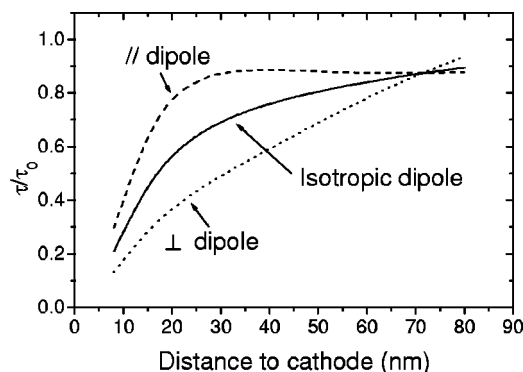
FIG. 3. Normalized lifetime vs exciton distance to cathode in the OLED (soda lime glass/100 nm ITO/40 nm PVK/80 nm Alq$_3$/Ag).

dipole and the metal cathode. The QM microcavity treatment provides an accurate description of the far-field radiative modes, but does not take into account this energy transfer to the cathode, which can dramatically increase the total decay rate W_{TOT}. In the absence of the microcavity, a dipole placed close to a metal surface sees an energy transfer rate in the form of $W_{ET} \propto l^{-3}$ in the limit of short dipole–cathode separation $l \ll \lambda$.[14–16] Although the effect of the cathode is expected to remain preeminent for a dipole in the OLED weak microcavity, the other dielectric interfaces also affect the field distribution in the microcavity; therefore, a more complete analysis is required for an exact solution. We use a Green's function formalism, taking into consideration the complex permittivity of the metal cathode. The readers are referred to Refs. 14 and 33 for detailed derivations. The normalized lifetime $\tau/\tau_0 = W_0/W_{TOT}$ [$\tau_0 = 1/(W_0 + W_{NR})$ is the PL lifetime] is plotted in Fig. 3 as a function of the dipole–cathode distance and the dipole orientation for a given OLED cavity. At a short distance away, the interaction between the near field of the dipole and the metal leads to a

high W_{ET}, i.e., cathode quenching, resulting in a very short lifetime. The rate of energy transfer is twice as fast for a perpendicular dipole as for a parallel dipole, the physics of which is similar to the radiation of dipole antennas immediately above the earth's surface.[34] The same principle was used to determine the orientation of single molecules at an interface by their fluorescence lifetimes.[35] In evaporated Alq$_3$ films, the molecular orientation is random, thus the ensemble average is isotropic. In polymer OLEDs, a preferred dipole orientation may exist due to spin coating of the polymer layer.[13,36,37] In this example, W_{ET} decreases rapidly with increasing dipole–cathode distance and the lifetime levels off to approximately 90% of the intrinsic lifetime at a dipole–cathode separation of 80 nm (cf. Ref. 22).

F. Selected numerical results

The results of the CCQMM model are significant departures from the classical theory as illustrated in the radial plot of modal intensity versus the mode angle in Alq$_3$. Figure 4(a) depicts the classical model, in which the TE and TM radiations are identical and isotropic, and the modes are delineated by the critical angles for TIR at the glass/air and ITO/glass interfaces. The total emitted flux is given by

$$F = 2\pi \int I(\theta)\sin\theta \, d\theta \qquad (7)$$

for an angular intensity pattern, $I(\theta)$. The emission at large angles to normal is heavily weighted because of the large solid angles corresponding to large θ, so much so that 47% of the emitted light is in the ITO/organic mode according to ray optics. In reality, the cutoff wavelength of the thin ITO/organic waveguiding slab may fall within the visible region, and the strength of the ITO/organic modes are in general less than what the classical theory leads one to believe.
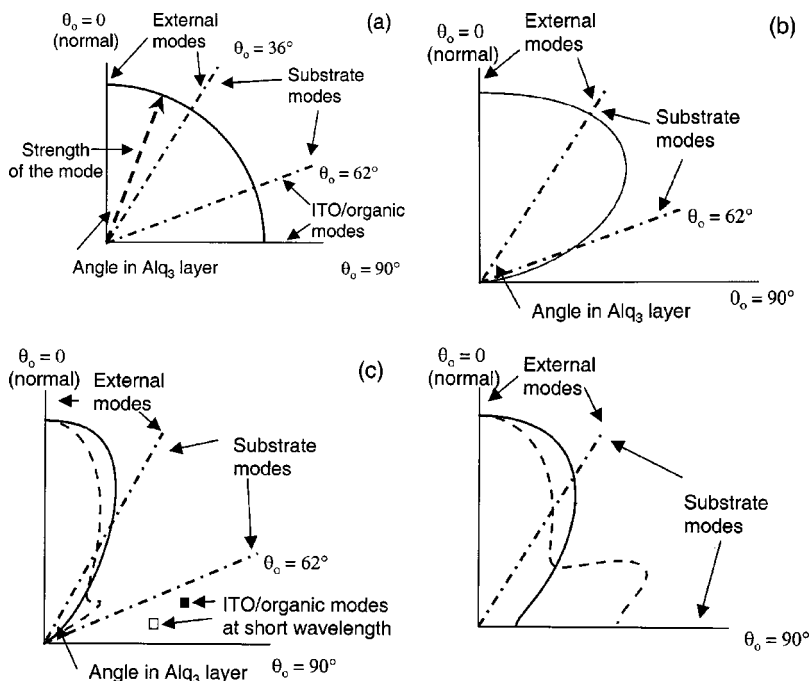

FIG. 4. Radial plots of modal strength (intensity) vs mode angle in Alq$_3$: (a) classical ray optics, (b) CCQMM model for an OLED with the structure: soda lime glass/100 nm ITO/40 nm PVK/80 nm Alq3/cathode, (c) the same OLED as in (b) except on high-index glass substrate. In (b) and (c), solid line: TE emission, dashed line: TM emission, the wavelength is 524 nm.

Wave optics is employed in the half-space dipole model, where the exciton in the OLED is approximated by a dipole located in a semi-infinite region of organic material on top of a semi-infinite metal cathode.[13] Figure 4(b) shows the same radial plot calculated by the half space dipole model:[13]

$$I(\theta) \propto |1+r_s \exp(i2\delta\cos\theta)|^2 + |1-r_p \exp(i2\delta\cos\theta)|^2, \tag{8}$$

where $\delta = 2\pi n_{org} l/\lambda$ is the phase distance from the cathode, and r_s and r_p are the Fresnel reflection coefficients for TE and TM waves, respectively. The intensity in the normal direction $I(\theta=0)$ has maxima at $\delta=(m+1/2)\pi$ or $l=(m/2+1/4)\lambda/n_{org}$. For the EL spectrum peak of 524 nm, the first maximum is located 77 nm from the cathode. In Fig. 4(b), the radiation is concentrated in the forward direction because the dipole–cathode distance of 80 nm is close to the first maximum. It should be noted, however, at other dipole–cathode separations, the half-space dipole model still predicts a large amount of radiation into the ITO/organic angle modes regardless of the actual OLED layer structure.

The results of the CCQMM model for a device with an 80-nm-thick Alq_3 layer at the peak emission wavelength ($\lambda=524$ nm) is shown in Fig. 4(c). The exciton is assumed to be residing at the PVK/Alq_3 interface, which is in close proximity to the antinode in the electric field (defined the same way as the maxima in the half-space dipole model above, ~77 nm from the cathode) at which point the TE and antinodal TM emissions are maximized [see Eq. (8) and discussions thereafter]. The radiation pattern retains much of the characteristics of that of an in-plane dipole again due to the fact that the electric field vector of both the TE and the antinodal TM waves are in the $x-y$ plane. The external and substrate modes form a continuum, because modal density is inversely proportional to the thickness of the region of space that the modes occupy. ITO/organic modes may exist at shorter wavelengths, but only as discrete modes. However, the energy in them may still be significant due to spatial confinement.

In an OLED on standard soda lime glass substrates, the ITO/organic modes are confined by TIR at the ITO/glass interface due to index mismatch between the substrate and the emitting layer ($n_{glass1} < n_{Alq}$). With the use of high-index substrates ($n_{glass2} > n_{Alq}$), the ITO/organic modes are converted into substrate-waveguided modes that exist predominantly in the substrate. Although the far-field intensity pattern of a planar OLED is independent of the index of the substrate, high-index substrates have been show to facilitate light extraction by substrate patterning techniques.[27] Figure 4(d) shows the radial plot of intensity versus mode angle in the device as in Fig. 4(d), except on a high-index substrate. The ITO/organic modes are no longer present, and all modes form a continuum. The radiation pattern resembles that of an in-plane dipole up to large angles from the normal, where interference effects from the ITO/organic layer on the TM radiation is observed.

III. EXPERIMENT

Bilayer OLEDs were fabricated on either 0.7-mm-thick soda lime glass substrates coated with ITO ($t_{ITO}=180$ nm,
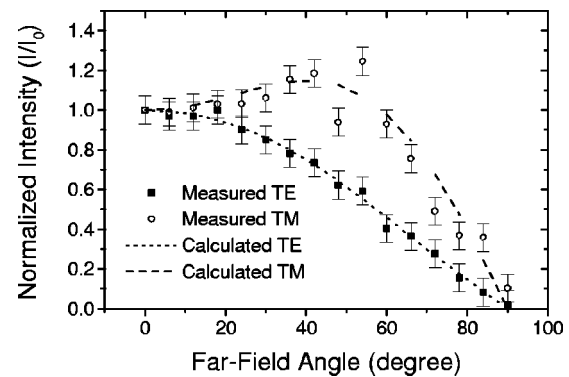

FIG. 5. Modeling and experimental data of far-field intensity pattern of a planar OLED (soda lime glass/180 nm ITO/40 nm PVK/20 nm Alq_3/Mg:Ag) (solid square and upper triangle) measured TE and TM intensity and (solid and dashed lines) theory.

$n_{ITO}=1.8$) purchased from Applied Films Corporation, or on bare 0.5-mm-thick soda lime or high-index glass substrates. 100 or 200 nm thick ITO layers ($n_{ITO}=2.0$) were deposited onto the bare glass substrates by rf magnetron sputtering in an Ar plasma with no intentional heating. The sheet resistance of the 100-nm-thick ITO was approximately 100 Ω/sq, and the transmission was ~80% in the visible. The hole transport layer in all devices was a 40 nm layer of PVK, deposited by spin coating from a PVK/Chlorobezene solution after the ITO surface was treated by an O_2 plasma.[38] The electron transport and emitting layer in all devices was Alq_3, deposited by vacuum sublimation at pressures $<10^{-6}$ Torr. The deposition rate was 0.1–0.3 nm/s. The cathodes were 30–50 nm of Mg:Ag (10:1) followed by an Ag cap evaporated through a shadow mask with 0.5-mm-diam holes. All lenses used for effective substrate shaping have a radius of curvature of 2.0 mm and a height of 1.5 mm, placing the OLED center exactly at the center of the curvature. They were made from the same material as the substrates, and were attached to the backside of the substrate with index-matching oil. All devices were driven at a current density of 10 mA/cm². Far-field light emission was detected by a Si photodiode on a stage with azimuthal rotation.

For the edge emission experiments, the substrate was diced, and the edges were vertical but not polished, so they acted as a diffusive scatterer. The edge emission was measured by another Si photodiode placed immediately adjacent to the substrate. This photodiode was covered with black tape except for a thin slit to prevent stray surface emission from interfering with the measurement.

IV. RESULTS AND DISCUSSION

A. Devices on planar substrates

The far-field intensity profiles from devices with thicker Alq_3 layers (40–80 nm) are qualitatively similar to the Lambertian profile, as has been observed in polymer LEDs elsewhere.[2,13,26] The exception was the device with a thin Alq_3 layer, where a significant peak in the intensity is observed in the TM polarized light (Fig. 5). In the thin Alq_3 layer, all excitons are close to the metal surface where in-plane TM radiation dominates as discussed following Eq.
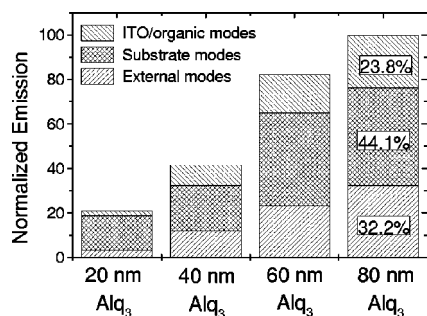
FIG. 6. Calculated distribution of radiative emission into external, substrate, and ITO/organic modes as a function of Alq$_3$ thickness for OLEDs with the structure soda lime glass/180 nm ITO/40 nm PVK/Alq$_3$/cathode.
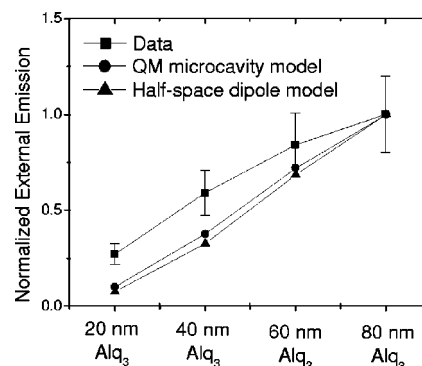

FIG. 7. Normalized external emission vs thickness of the Alq$_3$ layer: (squares) data, (circles) QM microcavity theory, and (up triangles) half-space dipole model. The devices are of the structure soda lime glass/180 nm ITO/40 nm PVK/Alq$_3$/Mg:Ag/Ag. The lines are guides to the eye only.

(5). This coupled with the transmission at the glass/air interface, which falls off at large angles, produced the peak in the TM intensity profile. The model results are in excellent agreement with the data.

By integrating or summing $I(\theta)$ [cf., Eq. (7)] over the appropriate ranges: $0 - \theta_{c1} = \sin^{-1} n_{air}/n_{Alq}$ for external modes, etc., we can compute the proportion of the internally generated emission that goes into each mode. First, we examine the emission as a function of the thickness of the Alq$_3$ layer for OLEDs on standard glass substrates (Fig. 6).[39] The overall height of the columns represents the rate of radiative decay W_R. The sharp decrease in radiative output with Alq$_3$ layer thickness can be attributed primarily to the cathode quenching effect. In the device with 80 nm Alq$_3$, the excitons are close to the antinode of the electric field in the microcavity, where according to Eq. (5), both the TE and antinodal TM contributions are maximized, leading to a large external and total emission. In contrast, in the device with 20 nm Alq$_3$, the excitons are close to the metal surface where the nodal TM contribution at large angles dominates. The large-angle radiation suffers from TIR resulting in far less external emission as a percentage of the total radiation. It should be pointed out that in the 80 nm Alq$_3$ device roughly one third of the emission is into the external modes, much greater than the 18.9% figure according to classical ray optics.

The external emission in the forward half plane of a series of OLEDs on standard substrates with the Alq$_3$ layer ranging from 20 to 80 nm was computed by integrating the measured intensity profiles according to Eq. (6). The normalized external quantum efficiency (photon/electron) as a function of the thickness of the Alq$_3$ layer is plotted in Fig. 7 along with the calculated values by both the CCQMM model and the half-space dipole model.[13] The external quantum efficiencies decrease with decreasing Alq$_3$ thickness due to cathode quenching as expected; however, both models underpredict the efficiencies in devices with thinner Alq$_3$ layers, while the CCQMM model is slightly more accurate. We attribute this misfit to the fact that a thinner Alq$_3$ layer increases the amount of electron current proportionally relative to that of holes, thus improving the carrier balance, making the device more efficient.[40] An alternative explanation is that the characteristic length of the exciton recombination profile lengthens with increasing Alq$_3$ thickness, which means the

average exciton recombination site is farther away from the cathode than assumed. By the same cathode quenching argument, we would expect the actual external emission to be more than the modeling results.

The thickness of the ITO layer affects the modal distribution in two ways. It alters the ITO/organic modes by changing the combined thickness of the ITO/organic layer and the external and substrate modes through interference effects. It is possible to have an ITO layer so thin that no ITO/organic mode exists for most of the visible spectrum. In the same vein as in Fig. 6, the distribution of light emission is calculated for OLEDs with 100-nm and 200-nm-thick ITO layers (Fig. 8). The emission into the ITO/organic modes in the OLED with the thinner ITO layer is drastically suppressed, since the cutoff wavelength is only slightly above the low end of the visible spectrum. On the other hand, the cutoff is above the peak emission wavelength of Alq$_3$ in the OLED with the 200 nm ITO layer, resulting in much stronger ITO/organic modes. The absolute value of the emission into the external and substrate modes is moderately affected by the interference effects, but not enough to prevent the proportion of external emission from increasing with decreasing ITO layer thickness. According to our model, as much as
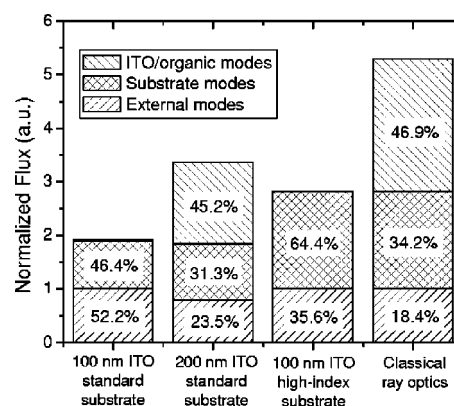

FIG. 8. Calculated distribution of emission into external, substrate, and ITO/organic modes for various OLED structures (glass substrate/ITO/40 nm PVK/80 nm Alq$_3$/cathode). The fluxes into the external modes of the sample with 80 nm Alq$_3$ on standard substrates and the classical model are normalized to 1.

TABLE I. Summary of increases in luminous flux for OLEDs on standard and high-index substrates after attaching a lens to the backside of the substrate.

	Standard glass		High-index glass	
	Theo.	Expt.	Theo.	Expt.
Q.E. for planar device[a]	N/A	0.35%	N/A	0.36%
Flux increase in forward half space	1.82×	1.5×	2.62×	2.3×
Flux increase in forward 120° cone	1.82×	1.7×	3.20×	2.9×

[a]Quantum efficiency (external photon/electron) is the same for both types of devices as measured from a group of large-area planar OLEDs.

~52% of the light could be emitted externally in the planar device with 100 nm ITO. External coupling efficiencies of more than 40% have been calculated by other groups.[14,18]

The use of high-index substrates eliminates TIR at the ITO/glass interface, which also converts the ITO/organic modes into substrate modes. From ray optics, we expect the external emission to be independent of the index of the substrate. This is confirmed by the measured external quantum efficiency of identically fabricated OLEDs on both soda lime and high-index glass substrates (Table I), as well as the observed far-field intensity profile (Fig. 9). The distribution of light emission for an OLED on high-index substrates is shown in Fig. 8 with the external emission normalized to that of an identical device on soda lime glass substrates. By converting the ITO/organic modes the device on the high-index substrate has more emission in the substrate modes and a higher total radiative output.

B. Devices on shaped substrates

Figure 9 shows the far-field intensity pattern of an OLED with an 80 nm Alq$_3$ layer on both standard and high-index substrates, with and without a lens attached. In devices
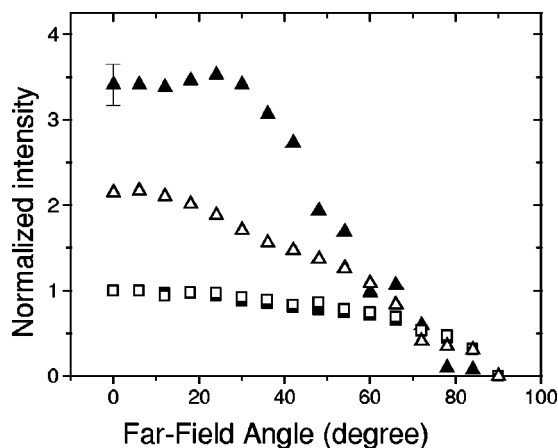

FIG. 9. Far-field intensity profile of OLEDs (glass substrate/100 nm ITO/40 nm PVK/80 nm Alq$_3$/Mg:Ag) on both high-index and standard glass substrates: (open and closed squares) planar soda lime and high-index glass substrates, (open triangles) shaped soda lime glass substrate, and (closed triangles) shaped high-index substrate.
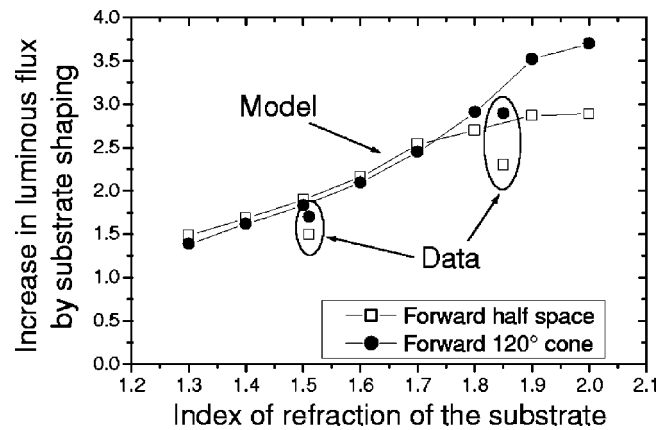

FIG. 10. Predicted increases in luminous flux emitted in the forward half plane and the forward 120° cone as a function of the index of refraction of the substrate, assuming complete conversion of substrate modes into external modes. OLEDs have the structure: substrate/100 nm ITO/40 nm PVK/80 nm Alq$_3$/cathode.

fabricated on planar substrates, the far-field intensity patterns are the same, irrespective of the index of the substrates, as expected. Once a lens of the same index as the substrate is attached, the devices on the high-index substrates showed an average increase by a factor of 3.2 in the intensity in the normal direction versus an average increase by a factor of only 2.2 for the devices on the standard substrates. These results are very close to the ideal scenario where the OLED is a point source at the center of curvature of the lens, where the expected increase is given by n_{glass}^2, i.e., by factors of 3.4 and 2.3 for high-index and standard glass substrates, respectively.

High-index substrates not only convert the ITO/organic modes, but also have a focusing effect on the distribution of emitted light rays. With a large substrate index ($n_{glass2} = 1.85$), diffraction from the emitting layer ($n_{Alq} = 1.71$) bends light rays forward in the substrate. In the ideal scenario where the OLED is a point source at the center of the curvature of the lens, the far-field intensity pattern in air is identical to the ray distribution in the substrate, so the emission in air is also more concentrated in the normal direction. If we were to look at the light emission in the forward 120° cone, where most of the viewing takes place, the amount of increase in external quantum efficiency is even more remarkable. The observed increase was by a factor of 2.9 for the device on a high-index substrate, and only a factor of 1.7 for the corresponding device on a standard substrate. Our model predictions of the increase in the forward half plane and 120° cone for both types of substrates agree well with the data. The discrepancy between theoretical and experimental values can be attributed to the finite size of the OLEDs and the imperfections at the edge of the lenses (Table I).

We also calculated the expected increase in the external luminous flux by attaching a lens with the same index as the substrate, assuming the same lens and OLED dimensions (Fig. 10). The predicted enhancement factor increases monotonically with the index of refraction of the substrate. As the index of the substrate increases beyond that of the emitting layer ($n_{Alq} = 1.71$), emission becomes more concentrated in

TABLE II. Measured values of $\eta_{cp}^{ext}/\eta_{cp}^{sub}$ compared with the calculations based on the CCQMM model and ray optics for different device structures. The thicknesses of the PVK and Alq$_3$ layers are 40 and 80 nm, respectively.

Sample	Measured	Model
Soda lime glass/100 nm ITO/PVK/Alq$_3$/Mg:Ag/Ag	1.30±0.20	1.12
Soda lime glass/200 nm ITO/PVK/Alq$_3$/Mg:Ag/Ag	0.51±0.08	0.75
High-index glass/100 nm ITO/PVK/Alq$_3$/Mg:Ag/Ag	0.41±0.06	0.56

the forward direction due to refraction. Hence for higher substrate indices, the luminous flux in the forward 120° cone shows a larger increase compared with that in the entire forward half space for higher substrate indices.

C. Edge emission measurement

Direct measurement of the substrate and ITO/organic waveguided light is difficult; therefore, we devised a method that indirectly measures the ratio of light emission into the external modes over that into the substrate modes, i.e., $\eta_{cp}^{ext}/\eta_{cp}^{sub}$.[42] A portion of the substrate waveguided light is made to emit externally by attaching a lens to the backside of the substrate. Due to the thickness of the substrate, it was assumed that attaching the lens negligibly affected the behavior of the OLED. Since the ITO/organic modes were heavily attenuated by the metal cathode and the absorption in the ITO layer, we assumed that the edge emission was exclusively composed of the substrate modes.[22] In the absence of scattering that mixes the modes, it follows that

$$F_{ext} + F_{sub} = F'_{ext} + F'_{sub} = r_1 F_{ext} + r_2 F_{sub},$$

$$\frac{\eta_{cp}^{ext}}{\eta_{cp}^{sub}} = \frac{F_{ext}}{F_{sub}} = \frac{1 - r_2}{r_1 - 1}, \qquad (9)$$

where F_{ext} and F_{sub} are the emissions in the external and substrate modes in a planar sample, and the primed symbols are the emissions after lens attachment. r_1 and r_2 are defined as F'_{ext}/F_{ext} and F'_{sub}/F_{sub}, respectively.

The measured ratios of $\eta_{cp}^{ext}/\eta_{cp}^{sub}$ for various devices are summarized in Table II. In the OLED with the structure: soda lime glass/100 nm ITO/40 nm PVK/80 nm Alq$_3$/Mg:Ag/Ag, our measurements indicated a $\eta_{cp}^{ext}/\eta_{cp}^{sub}$ ratio of 1.30±0.20. In other words, there is more emission into the external modes than the substrate modes. This is confirmed by our model, which predicted a ratio of 1.12. When the thickness of the ITO is increased to 200 nm, a $\eta_{cp}^{ext}/\eta_{cp}^{sub}$ ratio of 0.51 ±0.08 was obtained, indicating that emission into the substrate modes was almost twice that into the external modes. In the OLED on high-index substrates, the ITO/organic modes are redirected into the substrate modes; therefore, we can expect substantially less emission into the external modes than into the substrate modes. As expected, the data indicated a $\eta_{cp}^{ext}/\eta_{cp}^{sub}$ ratio of only 0.41±0.06. The model

predicted $\eta_{cp}^{ext}/\eta_{cp}^{sub}$ ratios of 0.75 and 0.56 for the device with thicker ITO and on high-index substrate, respectively. Although discrepancies between the data and the modeling results exist, there was a recognizable pattern that confirmed the reduction of emission into the external modes relative to the substrate modes as the ITO thickness was increased, and when high-index substrates were used. The agreement was reasonable despite the simplicity of our assumptions, chief among which is the lack of mode mixing scattering.

D. External efficiency optimization

It is clear from Fig. 7 that microcavity effects are at least as important as the transport of carriers in device optimization through layer thickness adjustments. Radiative emission is maximized for an exciton at an antinode of the electrical field in the cavity. For a perfect metallic cathode, the first antinode is a quarter wavelength away, or approximately 75 nm at the peak emission wavelength of Alq$_3$ ($\lambda \approx 524$ nm). Because the excitons diffuse away from the PVK/Alq$_3$ interface, the optimal Alq$_3$ thickness should slightly exceed $\lambda/4$. On the other hand, thick Alq$_3$ increases the operating voltage, so in practice the best power efficiency is obtained with Alq$_3$ thicknesses around 50 nm.[22] Further device improvement is possible if the external coupling can be decoupled from the charge transport.

There is a similar rule of thumb for the distance between the exciton and the dominant reflective interface (ITO/glass) on the anode side for optimizing external emission. That distance should be a multiple of half wavelength for maximum constructive interference of electrical fields at the point of the exciton (reflection at the ITO/glass interface contributes no phase change).[41] Again using the case of $\lambda \approx 524$ nm as an example the optimal ITO thickness is given by $d_{PVK}n_{PVK} + d_{ITO}n_{ITO} = \lambda/2$. The optimal ITO thickness according to this rule is found to be approximately 100 nm, assuming $d_{PVK} = 40$ nm, $n_{PVK} = 1.67$, and $n_{ITO} = 2.0$. Figure 11 plots $\eta_{exciton}$, η_{cp}^{ext}, $\eta_R = W_R/W_{TOT}$, and $\eta_{ET} = W_{ET}/W_{TOT}$ computed by the CCQMM model as a function of the ITO thickness for OLEDs on soda lime glass. The efficiencies are calculated for three material systems with $\eta_{PL} = 0.32$, 0.10, and 0.90. The out coupling efficiency η_{cp}^{ext} is independent of the nonradiative processes, thus is also independent of η_{PL}, and a peak value of 52.6% is observed at an ITO thickness of 100 nm as predicted by the simple rule of thumb noted above. But calculation of the distribution into the three radiative modes reveals that the suppression of ITO/organic modes due to the thinness of the ITO layer (Fig. 8) also plays a role. As the ITO thickness increases above 100 nm, ITO/organic modes start to contribute to the radiative decay and η_{cp}^{ext} decreases rapidly.

However, the more relevant parameter to device optimization is the number of photons emitted externally per singlet exciton $\eta_{exciton}$, which is a product of η_{cp}^{ext} and η_R. These efficiencies in Alq$_3$ ($\eta_{PL} = 0.32$) are plotted in Fig. 11(a). The total decay rate W_{TOT} does not change appreciably with the change in thickness of the ITO layer; however, the relative strength of the radiative decay and the dipole–cathode energy transfer depends sensitively on the ITO thickness.
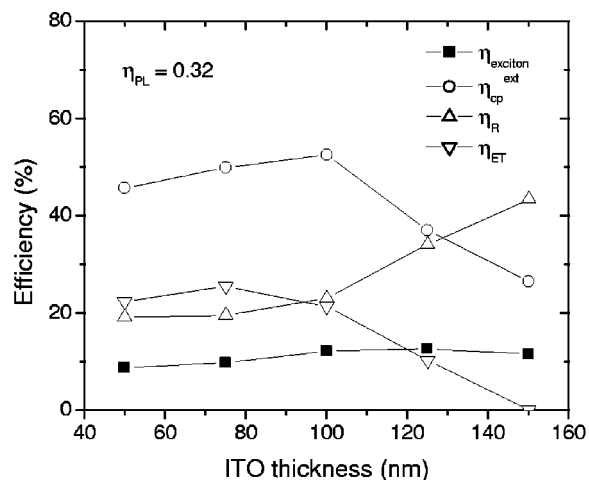
(a)
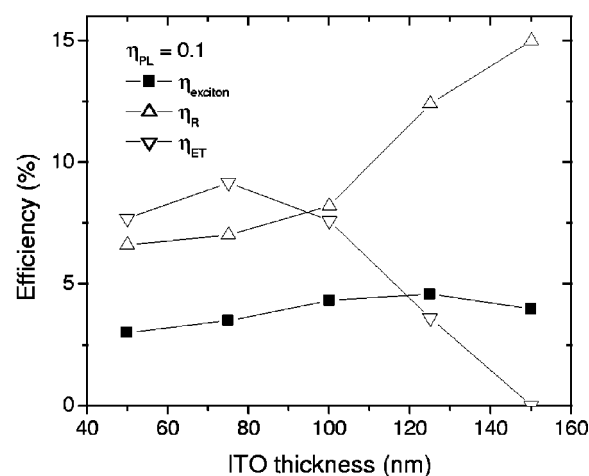
(b)
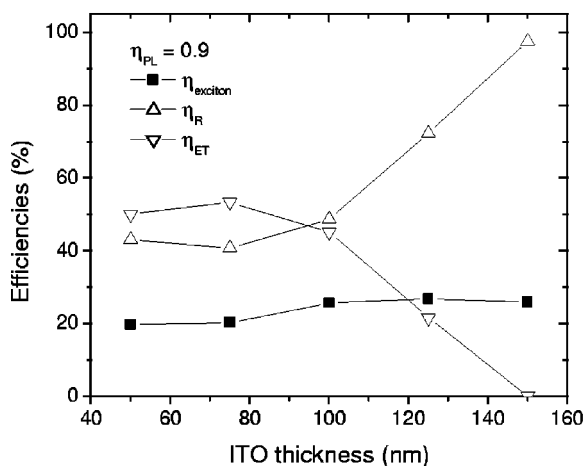
(c)

FIG. 11. (a) Various efficiencies vs ITO thickness calculated for OLEDs with the structure: soda lime glass/ITO/40 nm PVK/80 nm Alq$_3$/Ag: (closed quares) $\eta_{\text{exciton}} = W_{\text{ext}}/W_{\text{TOT}}$, (open circles) $\eta_{\text{cp}}^{\text{ext}} = W_{\text{ext}}/W_R$, (open up triangles) $\eta_R = W_R/W_{\text{TOT}}$, and (open down triangles) $\eta_{\text{ET}} = W_{\text{ET}}/W_{\text{TOT}}$. η_{PL} = 0.32 is used in the calculations. (b) and (c) The same efficiencies as in (a) with $\eta_{\text{PL}} = 0.10$ and 0.90, respectively. $\eta_{\text{cp}}^{\text{ext}}$ is the same in all three cases. The lines are guides to the eye only.
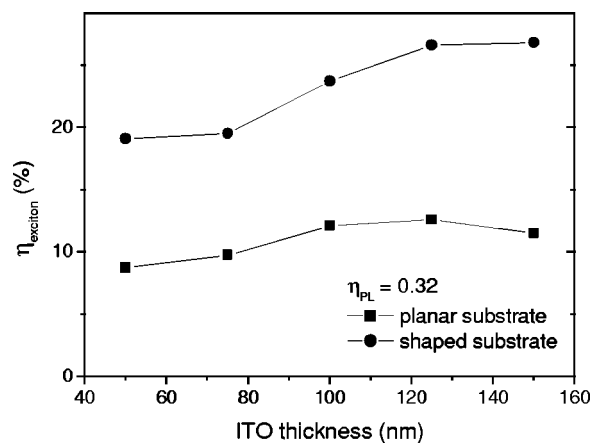

FIG. 12. Calculated η_{exciton} for OLEDs of the structure soda lime glass/ITO ($n_{\text{ITO}}=2.0$)/40 nm PVK/80 nm Alq$_3$/Ag where the intrinsic PL efficiency is 0.32: (squares) planar substrate and (circles) shaped substrate ($\beta=1$). The lines are guides to the eye only.

With a thicker ITO, the increase in the rate of radiative decay W_R, together with the decrease in dipole–cathode energy transfer W_{ET}, cause η_R to increase faster than the decrease in $\eta_{\text{cp}}^{\text{ext}}$, resulting in a notable increase in η_{exciton}. 125 nm of ITO gives the most efficient device on planar substrates where 12.6% of the singlet excitons emit a photon externally, whereas the device on 50 nm ITO is over 30% less efficient at $\eta_{\text{exciton}} = 8.7\%$. Some preliminary data affirm the model results, and will be published elsewhere. Material systems with an inefficient emitter ($\eta_{\text{PL}} = 0.10$) or an efficient emitter ($\eta_{\text{PL}} = 0.90$) are represented in Figs. 11(b) and 11(c). The absolute rate of decay for the radiative and the dipole–cathode energy transfer remain the same, although they now represent different fractions of the total decay rate. The devices on 125 nm ITO remain the most efficient devices predicted, where the η_{exciton}s are 4.6% and 26.7%, respectively. It remains likely that in some highly efficient devices ($\eta_{\text{PL}} \simeq 1$, $\eta_{\text{ET}} \simeq 0$), a high η_{exciton} can be achieved with thin ITO layers that eliminates the ITO/organic modes.

Figure 12 shows calculated η_{exciton} as a function of ITO thickness for OLEDs on both planar and shaped soda lime glass substrates. Shaped substrates ($\beta=1$) increase η_{exciton} by a factor of more than 2 compared with planar substrates as shown previously. Among the devices on planar substrates, the most efficient devices predicted is on 125 nm of ITO, whereas among the devices on shaped substrates, the most efficient device is on 150 nm of ITO ($\eta_{\text{exciton}} = 26.8\%$). The different ITO thickness alters the intensity distribution sufficiently that the optimization is dependent on whether the shaped substrate is used.

The highest η_{exciton} is obtained by using shaped high-index substrates. It converts ITO/organic modes (irrespective of the thickness of the ITO layer) into substrate modes which can be harvested by substrate patterning techniques. It also offers two advantages over the thin ITO/standard glass substrate combination. First, from an engineering point of view, high-index substrates allow a high conversion efficiency β for substrate features of the same size due to the favorable refraction of light rays that enter the substrate. Second, the

total radiative emission is higher in an OLED on a high-index substrate than on a thin ITO/standard glass substrate (Fig. 8), which translates into higher external emission in the presence of competing nonradiative processes.

V. CONCLUSIONS

We used a CCQMM model to describe the recombination of excitons in an OLED. The calculated emission rates into the external, substrate, and ITO/organic modes differ substantially for the classical ray optics result and are strong functions of the indices and thicknesses of the layers. We found that one of the chief shortcomings of the classical model is the failure to consider the cutoff effects of the ITO/organic waveguide. We found that external coupling efficiencies in excess of 50% is possible in certain structures. The model accurately predicted the far-field intensity pattern, the external/substrate mode ratio as determined by edge emission experiments, and the expected increase of external emission by employing shaped substrates. Finally, device optimization should aim to maximize the number of externally emitted photons per exciton of the appropriate type η_{exciton}, which we have calculated using the CCQMM model.

ACKNOWLEDGMENTS

[1] B. E. A. Saleh and M. C. Teich, *Fundamentals of Photonics* (Wiley, New York, 1991).

[2] N. C. Greenham, R. H. Friend, and D. D. C. Bradley, Adv. Mater. **6**, 491 (1994).

[3] T. Tsutsui, Mater. Res. Bull. **22**, 39 (1997).

[4] J. Kido and Y. Iizumi, Appl. Phys. Lett. **73**, 2721 (1998).

[5] T. Tsutsui, M.-J. Yang, M. Yahiro, K. Nakamura, T. Wantanabe, T. Tsuji, Y. Fukuda, T. Wakimoto, and S. Miyaguchi, Jpn. J. Appl. Phys., Part 2 **38**, L1502 (1999).

[6] M.-H. Lu, C. F. Madigan, and J. C. Sturm, Mater. Res. Soc. Symp. Proc. **621**, Q3.7 (2000).

[7] S. Saito, T. Tsutsui, M. Erra, N. Takada, C. Adachi, Y. Hamada, and T. Wakimoto, Proc. SPIE **1910**, 212 (1993).

[8] V. Cirmova and D. Neher, J. Appl. Phys. **79**, 3299 (1996).

[9] D. G. Lidzey, M. A. Pate, D. M. Whittaker, D. D. C. Bradley, M. S. Weaver, A. A. Fisher, and M. S. Skolnick, Chem. Phys. Lett. **263**, 655 (1996).

[10] J. Gruner, F. Cacialli, and R. H. Friend, J. Appl. Phys. **80**, 207 (1996).

[11] H. F. Wittman, J. Gruner, R. H. Friend, G. W. C. Spencer, S. C. Moratti, and A. B. Holmes, Adv. Mater. **7**, 541 (1995).

[12] H. Becker, S. E. Burns, and R. H. Friend, Phys. Rev. B **56**, 1893 (1997).

[13] J.-S. Kim, P. K. H. Ho, N. C. Greenham, and R. H. Friend, J. Appl. Phys. **88**, 1073 (2000).

[14] R. R. Chance, A. Prock, and R. Silbey, Adv. Chem. Phys. **37**, 1 (1978).

[15] R. R. Chance, A. Prock, and R. Silbey, J. Chem. Phys. **62**, 2245 (1975).

[16] R. R. Chance, A. H. Miller, A. Prock, and R. Silby, J. Chem. Phys. **63**, 1589 (1975).

[17] K. B. Kahen, Materials Research Society Fall Meeting, Boston, MA, Dec. 2000.

[18] N. Tessler, Appl. Phys. Lett. **77**, 1897 (2000).

[19] K. Ujihara, Phys. Rev. A **12**, 148 (1975).

[20] D. G. Deppe and C. Lei, J. Appl. Phys. **70**, 3443 (1991).

[21] G. Björk, S. Machida, Y. Yamamoto, and K. Igeta, Phys. Rev. A **44**, 669 (1991).

[22] V. Bulović, V. B. Khalfin, G. Gu, P. E. Burrows, D. Z. Garbuzov, and S. R. Forrest, Phys. Rev. B **58**, 3730 (1998).

[23] M. Pope and C. E. Swenberg, *Electronic Processes in Organic Crystals* (Oxford University Press, Oxford, 1982).

[24] D. Z. Garbuzov, V. Bulović, P. E. Burrows, and S. R. Forrest, Chem. Phys. Lett. **249**, 2009 (1996).

[25] Y. Cao, I. D. Parker, G. Yu, C. Zhang, and A. J. Heeger, Nature (London) **397**, 414 (1999).

[26] C. F. Madigan, M.-H. Lu, and J. C. Sturm, Appl. Phys. Lett. **76**, 1650 (2000).

[27] M.-H. Lu, C. F. Madigan, and J. C. Sturm, Tech. Dig. - Int. Electron Devices Meet. , 600 (2000).

[28] T. Yamasaki, K. Sumioka, and T. Tsutsui, Appl. Phys. Lett. **76**, 1243 (2000).

[29] G. Gu, D. Z. Garbuzov, P. E. Burrows, S. Venkatesh, and S. R. Forrest, Opt. Lett. **22**, 396 (1997).

[30] A. A. Shoustikov, Y. You, and M. E. Thompson, IEEE J. Sel. Top. Quantum Electron. **4**, 3 (1998).

[31] E. Hecht, *Optics*, 3rd ed. (Addison-Wesley, Reading, MA, 1998).

[32] C. W. Tang, S. A. van Slyke, and C. H. Chen, J. Appl. Phys. **65**, 3610 (1989).

[33] C. T. Tai, *Dyadic Green's Function in Electromagnetic Theory* (Intext, New York, 1971).

[34] A. Summerfeld, *Electrodynamics* (Academic, New York, 1952).

[35] J. J. Macklin, J. K. Trautman, T. D. Harris, and L. E. Brus, Science **272**, 255 (1996).

[36] Y. Shi, J. Liu, and Y. Yang, J. Appl. Phys. **87**, 4254 (2000).

[37] J. Liu, Y. Shi, L. Ma, and Y. Yang, J. Appl. Phys. **88**, 605 (2000).

[38] C.-C. Wu, C.-I. Wu, J. C. Sturm, and A. Kahn, Appl. Phys. Lett. **70**, 1348 (1997).

[39] The results presented in Figs. 6 and 8 are based on the lifetime calculated for each specific OLED rather than using the total decay rate calculated in Ref. 22. Thus they are more accurate than previously published results in Refs. 6 and 27, although the difference is small.

[40] H. Aziz, Z. D. Popovic, N.-X. Hu, A.-M. Hor, and G. Xu, Science **283**, 1900 (1999).

[41] T. Watanabe *et al.*, Synth. Met. **122**, 203 (2001).

[42] M.-H. Lu and J. C. Sturm, Appl. Phys. Lett. **78**, 1927 (2001).